

Article

Study of the Performance of Deep Learning Methods Used to Predict Tidal Current Movement

Kai Zhang ^{1,2} , Xiaoyong Wang ¹, He Wu ^{1,*}, Xuefeng Zhang ², Yizhou Fang ¹, Lianxin Zhang ³ and Haifeng Wang ¹

¹ National Ocean Technology Center, Tianjin 300112, China

² College of Ocean Science and Technology, Tianjin University, Tianjin 300072, China

³ National Marine Data and Information Service, Tianjin 300171, China

* Correspondence: wh_crane@163.com

Abstract: To predict tidal current movement accurately is essential in the process of tidal energy development. However, the existing methods have limits to meet the need for accuracy. Recently, artificial intelligence technology has been widely applied to solve this problem. In this paper, a tidal current prediction model combining numerical simulation with deep learning methods is proposed. It adopts three deep learning algorithms for comparative investigations: multilayer perceptron (MLP), long-short term memory (LSTM) and attention-ResNet neural network (AR-ANN). The numerical simulation was carried out using ROMS, and the observation collected in the Zhoushan region were used to validate the results. Compared with the numerical simulations, deep learning methods can increase the original correlation coefficient from 0.4 to over 0.8. In comparison, the AR-ANN model shows excellent performance in both the meridional and zonal components. This advantage of deep learning algorithms is extended in the tidal energy resource assessment process, with MLP, LSTM and AR-ANN models reducing the root mean square error by 32.9%, 34.4% and 42%, respectively. The new method can be used to accurately predict the hydrodynamic of tidal flow in the process of tidal energy extraction, which contributes to determine the suitable location for energy generation and tidal turbine design.

Keywords: deep learning; numerical simulation; tidal current prediction; tidal current energy assessment



Citation: Zhang, K.; Wang, X.; Wu, H.; Zhang, X.; Fang, Y. Zhang, L.; Wang, H. Study of the Performance of Deep Learning Methods Used to Predict Tidal Current Movement. *J. Mar. Sci. Eng.* **2023**, *11*, 26. <https://doi.org/10.3390/jmse11010026>

Academic Editors: Almudena Filgueira-Vizoso and Laura Castro-Santos

Received: 28 October 2022
Revised: 2 December 2022
Accepted: 6 December 2022
Published: 26 December 2022



Copyright: © 2022 by the authors. Licensee MDPI, Basel, Switzerland. This article is an open access article distributed under the terms and conditions of the Creative Commons Attribution (CC BY) license (<https://creativecommons.org/licenses/by/4.0/>).

1. Introduction

Marine renewable energy exploration is helpful to relieve the issues of environmental pollution and climate change [1]. As one kind of marine renewable energy, tidal current energy has been paid more and more attention by scientists and governments due to its strong regularity, excellent predictability, and high maturity [2,3].

Tidal currents are the periodic reciprocating horizontal movement of seawater caused by the celestial gravitational force. The kinetic energy of water flow is the tidal current energy, which can be converted into electrical energy as extracted by tidal turbines [4,5]. In the present stage of tidal current energy development, it is essential to improve the accuracy of energy prediction methods so as to determine the location and design of tidal turbines [6,7]. However, traditional forecasting methods are limited in meeting this need [8–10].

The existing tidal current prediction methods can be mainly classified into four types: statistical methods, dynamic models, artificial intelligence, and hybrid models.

Harmonic analysis, proposed by Professor G. H. Darwin, is the typical representation of statistical methods and was extensively applied in tidal current prediction in the early years. According to this method, tidal currents are regarded as the superposition of several sinusoidal waves with different frequencies [11]. Nonetheless, this simplifies the influence of the astronomical factors on tidal currents, neglects the random factors resulting in the turbulence, wind, and topographic conditions in actual situations, etc. [12,13].

Dynamical models consider the physical mechanism of flow movement and solve the control equations by means of numerical simulation. They simulate the periodic variation of the tidal current by taking a sufficient number of tidal constituents into account. In this way, they make up for the deficiencies of statistical methods to some extent [14]. However, their inaccuracy is still not able to meet the requirement of tidal current simulations currently. There is a deviation between the simulated and real values, which might be caused by numerous factors including imprecise model parameters, an ambiguous initial field, and various approximate conditions of the physical equations [15]. Hence, it is necessary to seek new solutions to improve the numerical models' performance.

With the advent of the big data era, more and more artificial intelligence methods have been introduced to ocean engineering. Ji Yao et al. [16] investigated the prediction of marine environmental loads considering the temporal correlation using long short-term memory (LSTM) neural networks, achieving higher accuracy and lower computational cost. A nonlinear mapping relationship between the marine environmental loads and float motions was also constructed using deep learning methods. Mohammad Najafzadeh and Giuseppe Oliveto [17] developed a machine learning (ML) model to achieve equations for predicting the propagation rate of scour around a pipeline caused by currents, based on various setup parameters and optimization strategies in the evolutionary and classification context. The equations given by the ML models provide reliable and physically consistent predictions of the scour propagation rate in comparison with scour tests. In a subsequent study, Mohammad Najafzadeh et al. [18] more intensively employed artificial intelligence (AI) models to derive new regression equations based on laboratory data to estimate the three-dimensional scour propagation patterns of submarine offshore pipelines exposed to the effects of currents and waves simultaneously. The model based on the proposed equations performs better than those reported in the literature.

This applied approach has also been extended to the field of tidal energy research [19]. As a branch of machine learning algorithms, deep learning methods are adept at automatically analyzing and extracting the change rules of tidal currents through the training process and use the learned rules to predict unknown data [20]. In terms of the complexity, periodicity, and nonlinear characteristics of tidal current variation, deep learning methods can overcome the weaknesses of existing statistical methods and numerical models [21–23].

Previous studies have proven the superiority of deep learning methods in tidal prediction and analysis. Amin Riazi et al. [24] proposed a new prediction method based on a multilayer perceptron network (MLP) for forecasting tidal height. It took the main factors resulting in tidal variations as the input, ensuring the physical validity and wide applicability of the prediction model. Cheng-hong Yang et al. [25] established a tidal water level prediction model based on LSTM applied to 17 ports in Taiwan, China. Compared with the differential autoregressive moving average model, support vector machine, and the particle swarm optimization method, the results showed that LSTM is superior to other models, with an advantage in time series prediction. It can effectively guarantee the prediction accuracy within 30 days, with an average root-mean-squared error of 0.049 m. Cihan Baymdir et al. [26] analyzed the feasibility of using the LSTM neural network to predict the meridional and zonal components of tidal current velocity. The results indicated that LSTM can effectively predict the change of tidal current velocity, and in addition, the performance is positively correlated with the length of time series during training. Dripta Sarkar et al. [27] used a Bayesian machine learning method to solve the spatio-temporal prediction of tidal flow changes. Compared with the traditional method using continuous observation data of a large number of locations, the method provides a better spatio-temporal description through integrating a mobile database and Gaussian process. Bo Feng et al. [28] proposed a tidal current prediction model considering the influence of multi-layer tidal current velocity. LSTM, MLP, and the Elman regression model were used to conduct comparative experiments. This work demonstrated that LSTM performed better than other traditional methods and significantly improved the prediction ability of tidal currents.

To date, many researchers have attempted to build hybrid models combining artificial intelligence and traditional methods. Abdollah Kavousi-Fard et al. [22] proposed a univariate prognostic approach based on the wavelet transform and support vector regression (SVR) to predict the tidal current speed and direction with high accuracy. The experimental results indicated the high capability and robustness of the proposed hybrid model for tidal current prediction. Hamed H.H. Aly et al. [29] proposed an intelligent optimized deep learning hybrid model based on the neural wavelet, Fourier series, and recursive Kalman filter for tidal flow prediction, in which the root-mean-squared error of the optimal hybrid model can be reduced to 0.047 m, achieving a high-precision prediction.

Most of the studies have been devoted to exploring the regional characteristics of currents and focused on making the best spatial predictions. Few works have implemented the analysis of tidal currents at a particular point in a certain ocean area, which is significant for tidal energy prediction and assessment. In the process of tidal energy extraction, the placement and operation of turbines at specific points would have an impact on the tidal variations. This category of error has been neglected in past tidal prediction methods, which would make a remarkable difference to the outcome of tidal energy assessment.

In this study, we propose a tidal current prediction model combining numerical simulation and deep learning to achieve the long-time prediction of tidal velocity and the high-accuracy evaluation of tidal energy. We argue that the deep learning method can effectively detect errors between numerical results and real values and then correct them. This advantage of the deep learning method will be amplified in the subsequent calculation of the tidal energy, which will result in a more accurate evaluation. The combination of the numerical model and deep learning methods has never been attempted in this field before, and the proposed model will provide a new way for tidal energy evaluation.

Considering the characteristics of different deep learning methods, there is still a need to discuss which method is more suitable for a particular situation. In previous studies, MLP and LSTM were the most frequently applied neural networks, but their suitability has not been analyzed. We propose a novel neural network, namely the attention-ResNet neural network (AR-ANN). By adding an attention mechanism to the ANN, this method attempts to improve the deviation of the tidal velocity in amplitude, which greatly affects the accurate calculation of the tidal energy. Therefore, the work in this paper will conduct comparative experiments on these three neural networks to find the optimal model while exploring the respective mechanisms.

The remainder of this paper is organized as follows. Section 2 introduces the overall structure of the proposed tidal current prediction model and the methods involved. In Section 3, comparative investigations of deep learning approaches for tidal current deviation correction are given by using tidal observation and simulation data. In Section 4, the corrected data are used to evaluate the tidal current energy and, then, verify the capability of the model. Finally, the conclusion and discussion are given at the end of this paper.

2. Methods

The tidal current prediction model proposed in this paper mainly consists of three parts, shown as follows:

1. To predict and analyze tidal current changes in target seas using a numerical model;
2. To construct neural networks based on simulation results and measurement data using different deep learning methods;
3. To calibrate tidal current velocity for non-observed periods using the neural networks above.

Firstly, the choice of the numerical model is crucial as the simulation results will provide a minimum guarantee for the tidal prediction. In view of the topographic characteristics and resolution requirements, the Regional Ocean Modeling System (ROMS) was chosen to simulate tidal currents.

Secondly, three different algorithms, multilayer perceptron (MLP), long-short term memory (LSTM), and the attention-ResNet neural network (AR-ANN), were built for

comparative experiments to analyze the performance. The model structures and network parameters were optimized and adjusted in the process of the experiments.

2.1. Numerical Model

The hydrodynamics of coasts, estuaries, and channels are the result of the interaction of currents with complex boundaries and water depths. Simulating tidal current in regions is a challenging task because of nonlinear processes, as well as the complex characteristics of topography. The Regional Ocean Modeling System (ROMS) was employed for this study to simulate the elements related to the tidal data.

The ROMS is a three-dimensional, terrain-following sigma-coordinate, nonlinear oblique pressure primitive equation model based on the Boussinesq and hydrostatic balance approximations. It can simulate movements at different scales, from global-scale oceanic circulation, mesoscale water level and flow field changes caused by astronomical tides, to small-scale coastal waters and other hydrological elements [30,31].

The main variables calculated by the ROMS model are three-dimensional water velocity, temperature, salinity, and free surface elevation. The physical formulation of the model is based on the mass and momentum conservation equations in the fluid, as well as the heat and salt transport equations. These equations, also known as the Navier–Stokes equations, describe the motion of a fluid and the relationship among the velocity, pressure, temperature, and density of the moving fluid. The standard Navier–Stokes equations used in the ROMS are listed below [32]:

The momentum equations:

$$\frac{\partial u}{\partial t} - fv + \vec{v} \cdot \nabla u = \frac{\partial \varphi}{\partial x} - \frac{\partial}{\partial z} (\overline{u'w'} - \nu \frac{\partial u}{\partial z}) + \mathcal{F}_u + \mathcal{D}_u \tag{1}$$

$$\frac{\partial v}{\partial t} + fu + \vec{v} \cdot \nabla v = \frac{\partial \varphi}{\partial x} - \frac{\partial}{\partial z} (\overline{v'w'} - \nu \frac{\partial v}{\partial z}) + \mathcal{F}_v + \mathcal{D}_v \tag{2}$$

The continuity equation:

$$\frac{\partial u}{\partial x} + \frac{\partial v}{\partial y} + \frac{\partial w}{\partial z} = 0 \tag{3}$$

The hydrostatic equation:

$$\frac{\partial \varphi}{\partial z} = \left(\frac{-g\rho}{\rho_0} \right) \tag{4}$$

The state equation:

$$\rho = \rho(T, S, P) \tag{5}$$

The transport equation:

$$\frac{\partial C}{\partial t} + \nabla \cdot (\vec{v}C) + \frac{\partial wC}{\partial z} = \frac{\partial}{\partial z} (\kappa \frac{\partial C}{\partial z}) + \mathcal{F}_C + \mathcal{D}_C \tag{6}$$

where $\nabla : (\frac{\partial}{\partial x}, \frac{\partial}{\partial y})$ is a horizontal gradient, (x, y) are the horizontal Cartesian coordinates, z is the vertical coordinate, positive upward, t is time, f is the Coriolis parameter, g is the acceleration of gravity, ν is the molecular viscosity, $\varphi(x, y, z, t)$ is the dynamic pressure, u, v, w are components of the vector velocity, C is a passive tracer concentration, $\mathcal{D}_u, \mathcal{D}_v, \mathcal{D}_C$ are diffusive terms, and $\mathcal{F}_u, \mathcal{F}_v, \mathcal{F}_C$ are forcing terms.

These equations are central to the ROMS numerical model for flow modeling, current variability, and the evolution of other natural fluid phenomena. By solving these equations numerically, the gridded data of the tidal velocity can be obtained.

2.2. Deep Learning Methods

As a branch of machine learning, deep learning is a semi-theoretical and semi-empirical modeling approach based on mathematical knowledge and computer algorithms. With the help of as much training data as possible and the large-scale computing power of computers, it will adjust the internal hyperparameters of neural networks in order to gradually approximate the problem objectives and learn nonlinear laws.

In recent studies, MLP and LSTM have been the most frequently used deep learning algorithms to predict tidal currents, with some success. In the process of tidal energy evaluation, the accuracy of the amplitude and phase of the tidal velocity is crucial. To address this feature, this paper proposes the AR-ANN algorithm, which improves the exact control of tidal velocity variation characteristics by adding an attention mechanism and a residual neural network to the ANN. The specific descriptions of the three neural networks are as follows.

2.2.1. Multilayer Perceptrons

Multilayer perceptrons (MLPs), also known as artificial neural networks (ANNs), are neural networks with at least one hidden layer. The basic structure of the feedforward neural network is shown in Figure 1. The first layer of the MLP is the input layer; the middle ones are the hidden layers; the last layer is the output layer. These layers are fully connected, and the output of each hidden layer is transformed by an activation function [33–35].

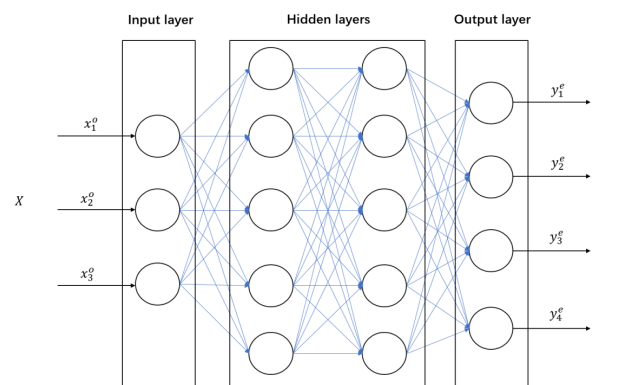


Figure 1. The structure of MLP.

During the process of training, the forward propagation algorithm is used to solve the output relation between two adjacent layers, which means the input of one layer is the output of the previous layer, and the back propagation algorithm is used to solve the coefficient relation matrix W , as well as the bias matrix B of each layer. Considering three hidden layers in the actual construction of the model, the equations of MLP can be described as follows:

$$Y = \sigma_3(W_3(\sigma_2(W_2(\sigma_1(W_1X + B_1)) + B_2)) + B_3) \tag{7}$$

where X is the input vector; Y is the output vector; σ_i is the activation function between layers; W_i and B_i represent the learnable weight and bias matrix, respectively.

It can be seen that, by nesting linear functions in multiple layers and providing a nonlinear modeling capability by the activation function, MLP can approximate any nonlinear function. Due to the simplicity of the network structure, it is used as a comparison standard to measure the performance of other deep learning algorithms.

2.2.2. Long Short-Term Memory Network

The long short-term memory network (LSTM) is a kind of recurrent neural network, which can capture the time characteristics and temporal dependence of long sequences by introducing memory and an oblivion gating system. Compared to the preceding feedfor-

ward neural networks, LSTM has the function of “memory”, embodied in the network as the previous information memory and applied to the calculation of the current output, to effectively solve the scheduling problem [36,37]. The equations are given as follows:

$$f_t = \sigma_g(W_f x_t + U_f x_{t-1} + b_f) \tag{8}$$

$$i_t = \sigma_g(W_i x_t + U_i h_{t-1} + b_i) \tag{9}$$

$$o_t = \sigma_g(W_o x_t + U_o h_{t-1} + b_o) \tag{10}$$

$$\tilde{c}_t = \tanh(W_c x_t + U_c h_{t-1} + b_c) \tag{11}$$

$$c_t = f_t \circ c_{t-1} + i_t \circ \tilde{c}_t \tag{12}$$

$$h_t = o_t \circ \tanh(c_t) \tag{13}$$

where f_t represents the activation vector of the forget gate of time t ; σ_g is the sigmoid activation function; o_t is the activation vector of the output gate; i_t is the activation vector of the input gate; $U_f, W_f, W_o, W_i, W_c, U_o, U_i,$ and U_c are the parameter matrices; \tilde{c}_t is the cell input activation vector; c_t is the cell state vector; b_f is the bias vector corresponding to the forget layer; \circ is the Hadamard product; h_t is the output vector of LSTM.

The neural network designed for the LSTM algorithm is shown in Figure 2. The input vector first passes through three blocks of the same structure. Every block contains an LSTM layer, dropout layer, and layer normalization. The dropout layer prevents overfitting by ignoring a certain number of neurons. The layer normalization prevents the gradient from exploding and disappearing by applying a normalization operation to the elements of each channel. The neural network ends with a fully connected layer, which is used to output the final prediction.

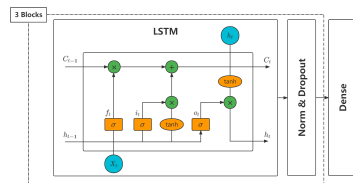


Figure 2. The structure of LSTM.

2.2.3. Attention-ResNet Neural Network

The attention mechanism captures important information by simulating the human brain allocating more attention to a certain part of a large amount of information at a certain moment in time. It is implemented by creating a query and a set of key–value pairs mapped to an output, where the query, key, value, and output are all vectors [38]. For a given input sequence $X \in R^{n \times d}$, where n is the sequence length and d is the embedding dimension, the output of a multihead attention layer is given as follows:

$$Q_i, K_i, V_i = XW_i^Q, XW_i^K, XW_i^V \tag{14}$$

$$\text{head}_i = \text{Attention}(Q_i, K_i, V_i) \tag{15}$$

$$= \text{Softmax}\left[\frac{Q_i K_i^T}{\sqrt{d_k}}\right] V_i \tag{16}$$

$$\text{MultiHead} = \text{Concat}(\text{head}_1, \dots, \text{head}_h) W^O \tag{17}$$

where $W_i^Q \in R^{d \times d_q}$, $W_i^K \in R^{d \times d_k}$, $W_i^V \in R^{d \times d_v}$, and $W_i^O \in R^{d_v \times d}$ are learnable projection matrices. For the multihead attention with h heads, it is a common manner to set $d_q = d_k = d_v = d/h$ to control parameter growth. It is worth mentioning that, in the solution of the temporal prediction problem, a mask is usually added to the attention mechanism, which is not involved in the designed neural network.

In this work, the specific architecture is shown in Figure 3. The input vector first goes through a multihead attention layer for feature extraction, followed by a residual neural network (ResNet) and layer normalization. ResNet is a deep network built by introducing residual blocks, which can reduce information loss and improve the convergence speed [39]. The final prediction is obtained through the following fully connected layer and dropout layer.

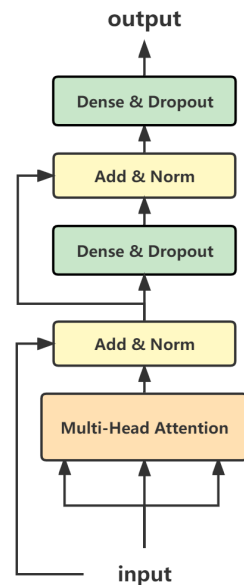


Figure 3. The architecture of AR-ANN.

3. Experiments

3.1. Numerical Simulation

3.1.1. Simulations

For this research, a nested domain with a bigger region (parent domain) embedding a smaller region (child domain) was designed (see the box bounded by the red line in Figure 4a) to resolve the impacts of complex coastlines and islands on the tidal currents. The resolution ratio of the parent domain was about 1 km, while that of the child domain containing the tidal observation data reached nearly 100 m.

The bathymetry field was taken from 15''-resolution GEBCO topography data and then smoothed with a smoothing parameter of no more than 0.2. The time step was 20 s for the parent domain and 4 s for the child domain. The model was driven by the harmonic constants of 8 major tidal constituents (semi-diurnal: M2, S2, N2, K2 and diurnal: K1, O1, P1, Q1); the data were obtained from TPXO. The open boundary conditions were set as follows: Chapman conditions for the free surface and Flather conditions for the 2D momentum. The amplitudes and phases of the eight tidal components were set at each node of the lateral open boundary in the parent domain, and their values vary spatially at each node. The influence of wind and other atmospheric factors was neglected.

In the model, the K-profile parameterization (KPP) scheme was used to compute the vertical mixing, and the bottom friction was approximated by the quadratic law. The simulated tidal currents in this region are very sensitive to the bottom drag coefficient, and several values were selected for a sensitivity test to find the optimal value: 0.0003, 0.0005, 0.001, 0.002, and 0.0025. After comparing the amplitude and phase of the M2 tide with the observations from the nine tidal gauge stations, the spatially uniform bottom drag coefficient was set to be 0.001 for the simulation. The model was run for a period of 38 days using the cold start method, and the last 35 days were used for the subsequent experiment. The tidal hydrodynamics was simulated in 2D mode, and the vertical mean tidal velocity was obtained in all nodes of the grid.

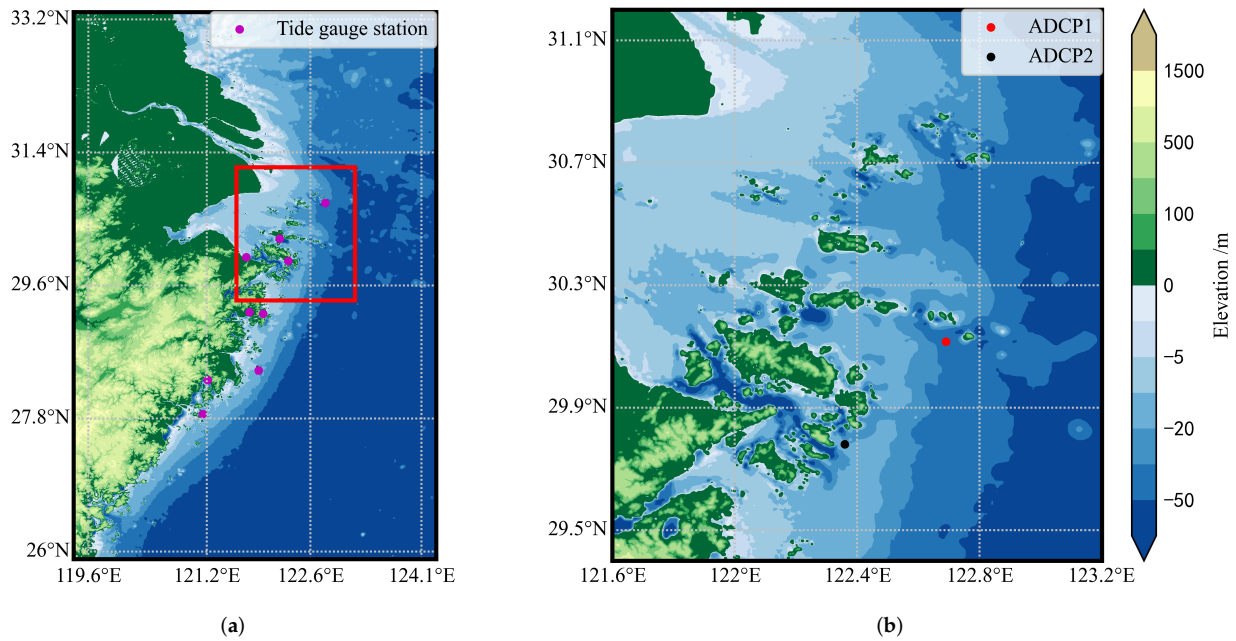


Figure 4. Spatial distributions of bathymetry in the simulated range of the ROMS in the Zhoushan sea. (a) The parent domain for the simulation. The pink dots indicate the locations of nine tidal gauge stations used for the model data validation. (b) The child domain for simulation, indicated by the red box in (a). The red dot indicates the placement of the observation equipment ADCP1 used for the corrected data validation in the subsequent experiment. The black dot indicates the location of ADCP2 used for model data validation.

3.1.2. Validation

The simulated results were compared against in situ observations for the amplitude and phase of the dominant harmonic constituents (M_2 and S_2) for the surface elevation change at the 9 long-term tidal gauge stations marked in Figure 4a. The amplitude and phase of the observations and models for the two components are given in Figure 5, and the root-mean-squared errors (RMSEs) were calculated for comparison as well.

It can be seen that the simulation results fit well the observation of the M_2 harmonic constituent both in amplitude and phase. The main difference is reflected in the S_2 harmonic constituent, with an RMSE of 0.134 m in amplitude and a consistent delay in phase, with an average deviation of 13.88°.

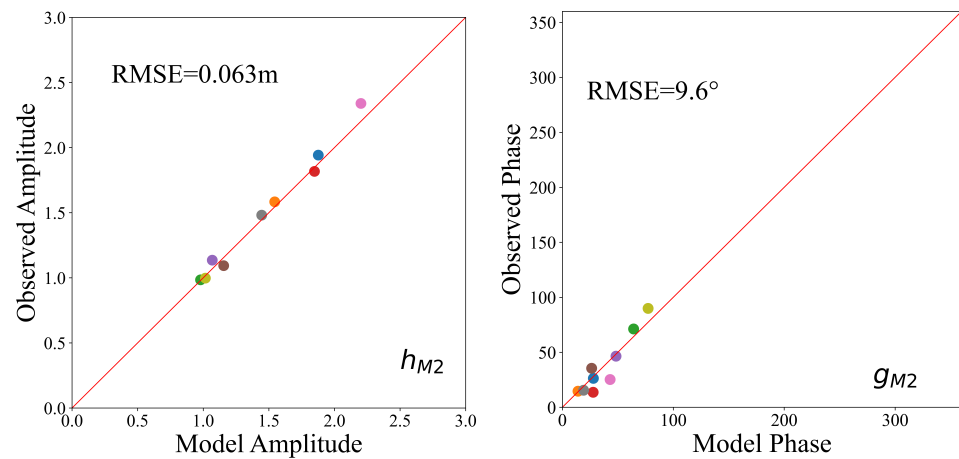


Figure 5. Cont.

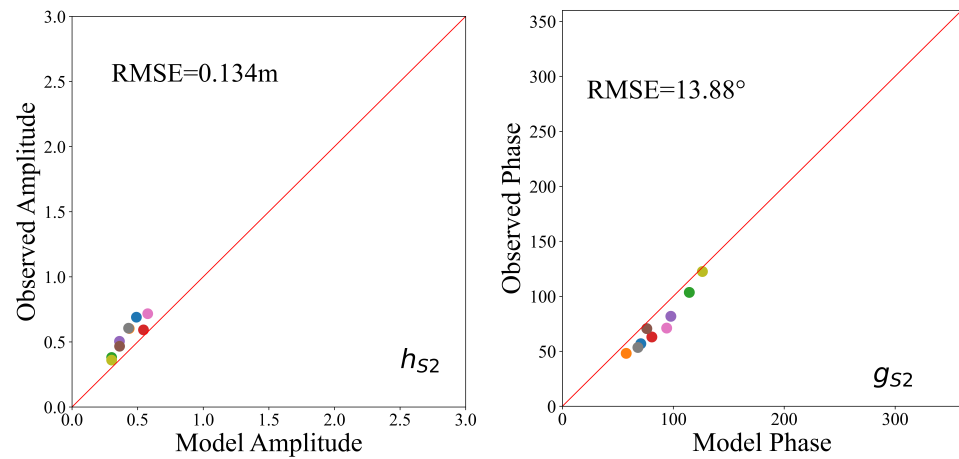
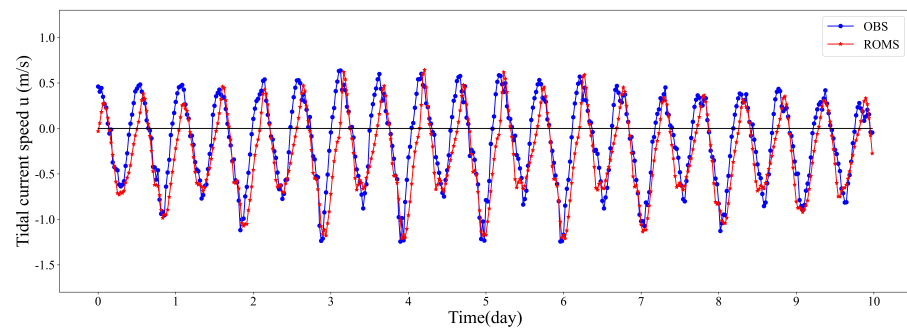
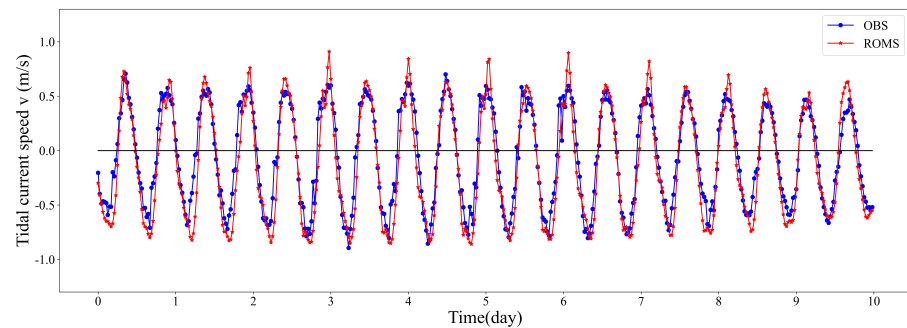


Figure 5. Regression analysis of the amplitude, h , and phase, g , for the M_2 and S_2 harmonic constituents.

We also used the measured data obtained from two ADCPs to verify the agreement in terms of tidal current velocity, and the locations of the two ADCPs are labeled in Figure 4b. The simulation from ADCP2 was in great agreement with the observed data, both in the longitudinal and latitudinal components. We selected 10 days of data and present the results in Figure 6. In contrast, the data deviation at ADCP1 was more pronounced, with a certain degree of difference in both amplitude and phase. Because of the longer duration of continuous data at ADCP1 and the necessity of tidal deviation revision, the observation from ADCP1 was elected for the subsequent research.



(a)



(b)

Figure 6. Comparison results of the tidal current speed from observation and the ROMS. (a) Comparison of the simulation data and actual value for u in ADCP2. (b) Comparison of the simulation data and actual value for v in ADCP2.

3.2. Experiment and Results

3.2.1. Datasets

The tidal current data were collected in Zhoushan, China. There was a consecutive observation of the velocity and the direction of the tidal current by using an acoustic Doppler current profiler (ADCP). The observation equipment was positioned at 122.690° E, 30.116° N, which is marked as the red dot shown in Figure 4. The measurement lasted from 30 May to 9 July 2021, and the tidal current data were recorded at a frequency of 10 min.

To improve the validity of the observations, the following quality control operations were performed after data collection: (1) remove obvious outliers such as sudden changes and (2) fill data gaps using smoothing methods. The zonal component u and meridional component v of the velocity were calculated.

To balance the model effectiveness and training cost, 12 consecutive hours of tidal velocity data were selected as a sample, which means the sequence length was 72. Therefore, we ended up with 5700 samples, of which the first 4400 were used for training, 4400–4700 for validation, and the last 1000 for testing. The simulated and measured data were used as the input and output for training the three different neural networks, respectively.

In order to optimize the performance and conduct comparative experiments, the optimal parameters for each proposed model were searched using the exhaustive method. The units for the dense and LSTM layers were selected from 100 to 400, each time increasing by 100, while the number of heads increased from 1 to 10 as well. The optimizer was the Adam algorithm, and the MSE was the loss function for all networks. Early stopping was used to avoid invalid training, and patience was defined as 20. More details about the parameters of the three networks are shown in Table 1.

Table 1. Detailed information for deep learning algorithms.

Parameter	MLP	LSTM	AR-ANN
Input Shape	(None,72)	(72,1)	(None,72)
Batch Size	100	100	100
LSTM Units	/	300/200/200	/
Dense Units	300/200/200	/	300/200
Head Numbers	/	/	6
Dropout Rate	0.3	0.3	0.3
Epoch	100	100	100

3.2.2. Performance and Model Validation

In order to validate and study the performance of the above-mentioned methods, the mean absolute error (MAE), the root-mean-squared error (RMSE), and correlation coefficient (R) were used to evaluate the accuracy, which are defined as follows:

$$MAE = \frac{1}{n} \sum_{i=1}^n |y_i - x_i| \tag{18}$$

$$RMSE = \sqrt{\frac{\sum_{i=1}^n (y_i - x_i)^2}{n}} \tag{19}$$

$$R = \frac{\sum_{i=1}^n (x_i - \bar{x})(y_i - \bar{y})}{\sqrt{(\sum_{i=1}^n (x_i - \bar{x})^2)(\sum_{i=1}^n (y_i - \bar{y})^2)}} \tag{20}$$

where n is the number of samples, x_i is the observed value at time i from the ADCP, and y_i is the estimated value at the same time from each model mentioned above, while \bar{x} is the average value of the measured data and \bar{y} is the average value of the estimated results.

To avoid serendipity, we first selected 10 samples randomly from the test set for evaluation. The corresponding RMSE and MAE results are shown in Figure 7. The simulations were in less agreement with the observation data, with u in the RMSE around 0.3 m/s, while the value of v in the RMSE was below 0.25 m/s. In the case of neural networks with identical parameters and training processes, this difference led to different calibration results.

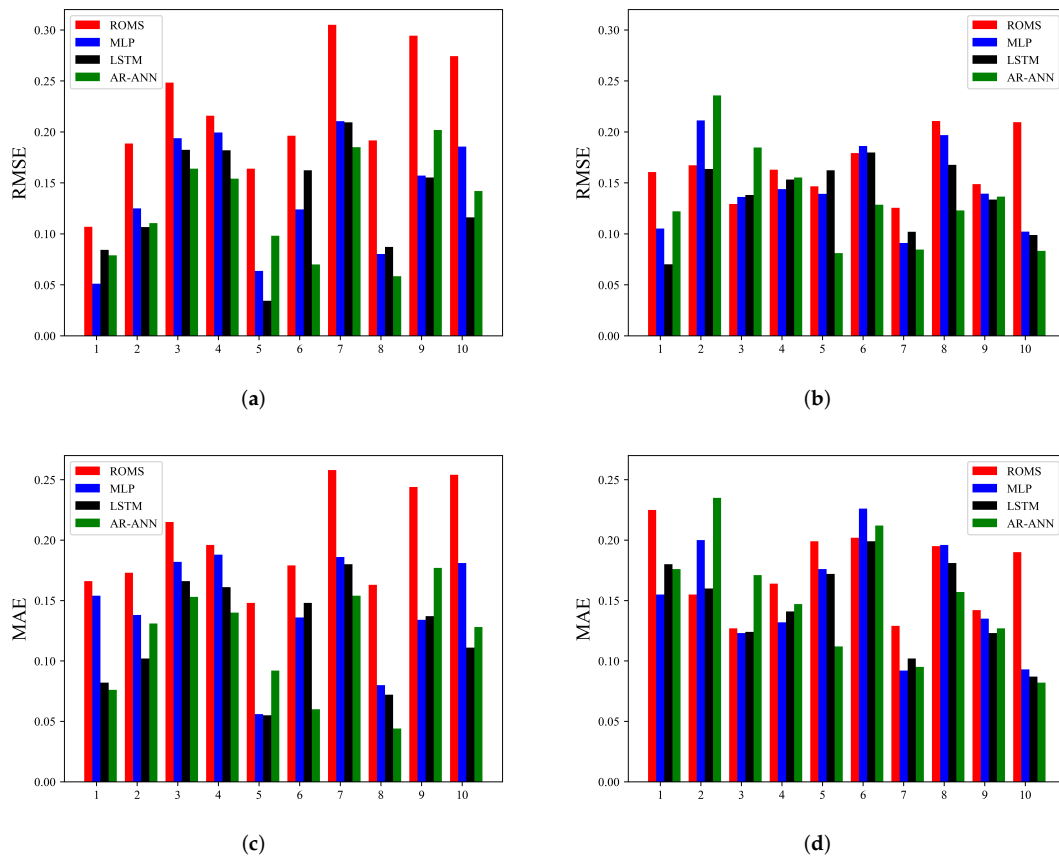


Figure 7. The evaluation metrics of the simulation and the three networks for the ten samples. (a) RMSE of simulation and corrected data for component u ; (b) RMSE of simulation and corrected data for component v ; (c) MAE of simulation and corrected data for component u ; (d) MAE of simulation and corrected data for component v .

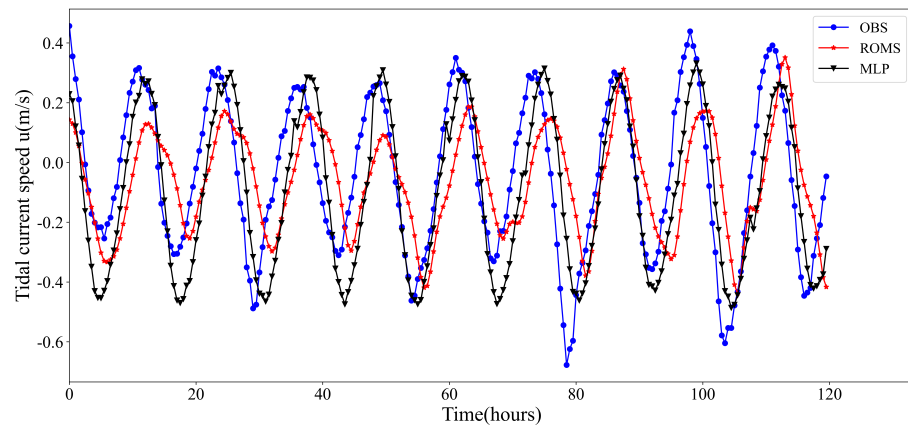
For component u , it can be seen that both the RMSE and MAE of the values corrected by the deep learning methods were smaller than those of the simulations, which indicates that the three built networks had different degrees of the correction effect. This further proves that deep learning methods can effectively reduce the simulation bias of the tidal velocity and improve the accuracy.

In the comparison of the three methods, we can find that the MLP model showed poor performance for individual samples, such as Samples 3 and 4, while it performed well for the others, indicating that the MLP model is not stable and lacks the ability to correct certain data with the characteristics. The AR-ANN and LSTM were able to calibrate all the samples and showed consistency in ones with different features.

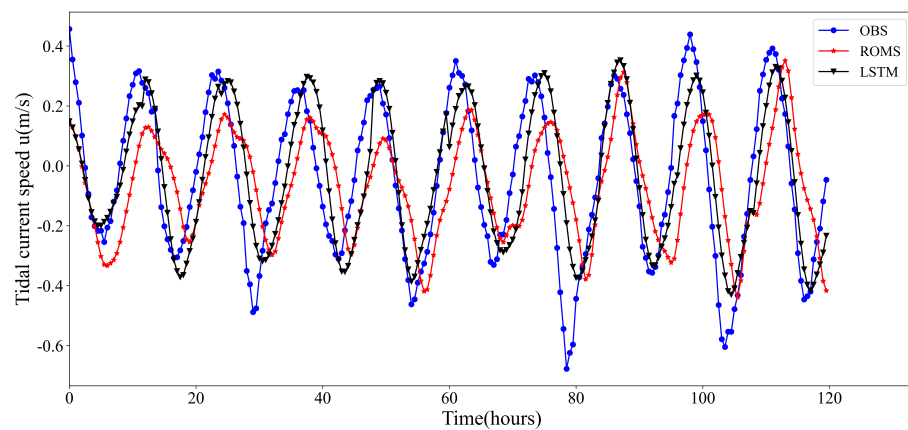
For component v , in the presence of larger biases in the original data, the deep learning approaches demonstrated superior correction capabilities, such as Samples 1, 8, and 10. In contrast, the deep learning methods did not work when there was a good agreement with the observed data, suggesting that there is an optimal correction limitation, which may be caused by errors in the observed values.

In order to explore the mechanism of the bias correction of various deep learning methods and to better evaluate the different models, the tidal velocity data of five consecutive

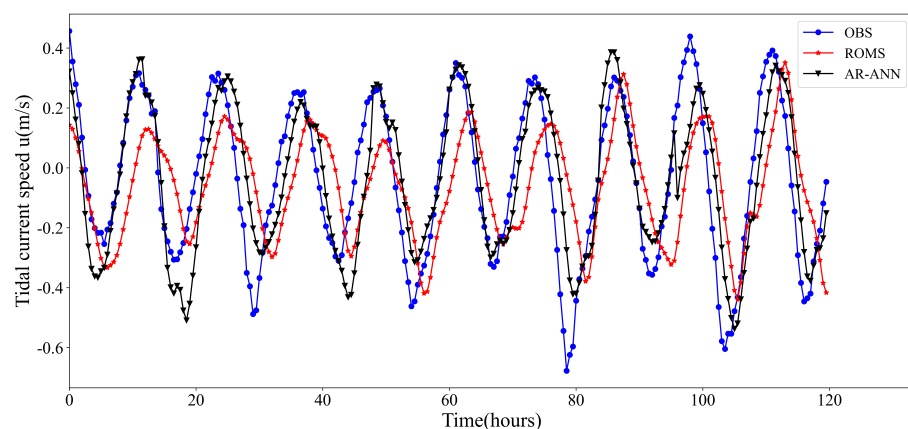
days were used and corrected by the three deep learning methods. The results are shown in Figures 8 and 9, and the calculated evaluation metrics are listed in Table 2 as well.



(a)



(b)

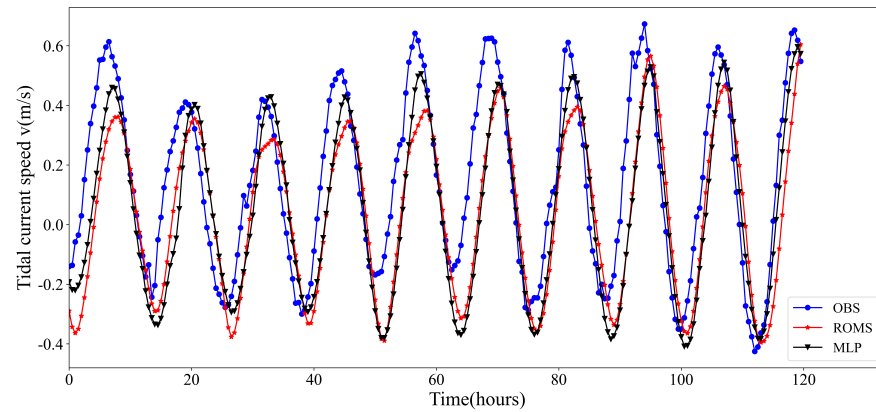


(c)

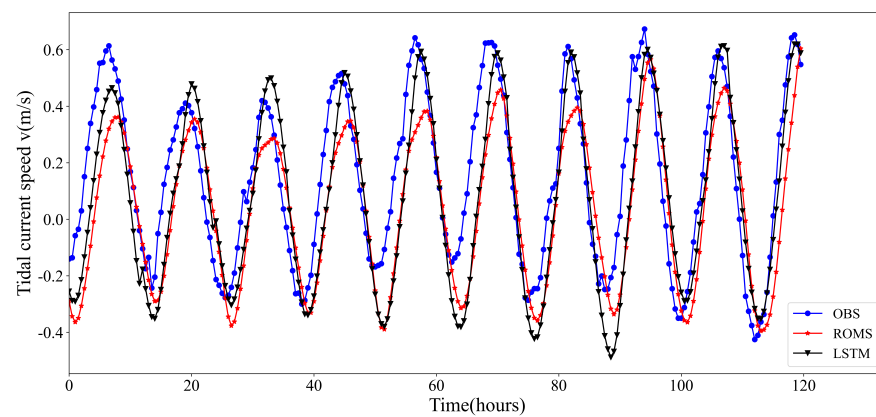
Figure 8. Comparison results of the tidal current speed bias correction by using the three machine learning algorithms. (a) Comparison of the MLP method, simulation data and actual value; (b) comparison of the LSTM method, simulation data and actual value; (c) comparison of the AR-ANN method, simulation data and actual value.

From the results of the simulations, it can be concluded that the deviations of the numerical model for tidal velocity mainly originated from both amplitude and phase. In

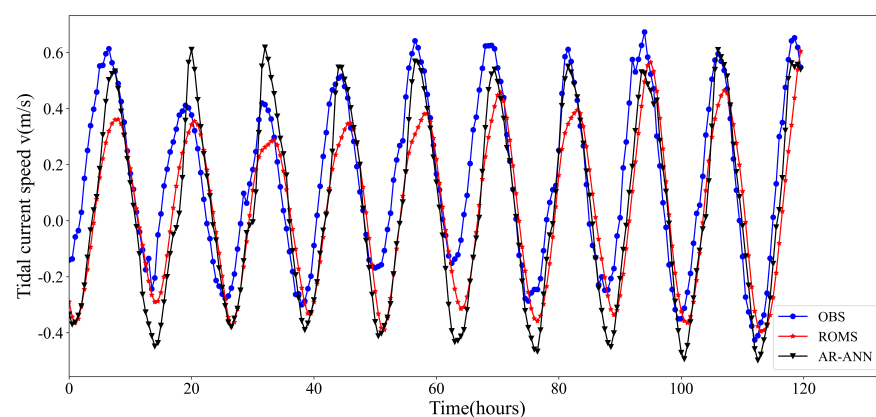
terms of components u and v , it can be clearly seen that the amplitude of the simulation data was significantly smaller than the observed data, and there was also a delayed misalignment in the phase. The accuracy of the amplitude and phase is crucial, and how to reduce these two biases is important to predict the tidal flow movements.



(a)



(b)



(c)

Figure 9. Comparison results of the tidal current speed bias correction by using the three machine learning algorithms. (a) Comparison of the MLP method, simulation data and actual value; (b) comparison of the LSTM method, simulation data and actual value; (c) comparison of the AR-ANN method, simulation data and actual value.

For component u , all three deep learning methods effectively corrected the simulation bias with very little variation from the observation. The main difference was that the MLP and AR-ANN models were more sensitive to the amplitude magnitude. However, the amplitude of the MLP model was significantly larger than that of the observed data, which is why the MLP model can have a high value of the MAE while a low value of the RMSE for several samples. The AR-ANN model also exhibited this similar phenomenon for the same reason.

The LSTM model showed superiority in the correction of the phase differences, but it was not significantly different from the simulation in terms of the amplitude. The limited correction ability for cases where the observed data were significantly lower than the simulated data is its shortcoming.

Table 2. Error metric for tidal current speed u .

Variable	Metric	ROMS	MLP	LSTM	AR-ANN
U	RMSE	0.234	0.160	0.150	0.146
	MAE	0.200	0.143	0.121	0.113
	R	0.484	0.811	0.820	0.830
V	RMSE	0.176	0.163	0.161	0.153
	MAE	0.173	0.153	0.147	0.152
	R	0.814	0.848	0.866	0.892

Overall, the RMSE and MAE values of MLP were higher than the other two neural networks, which means its performance is poor. In comparison, good results were obtained using the AR-ANN model, with the RMSE decreasing from 0.234 to 0.146, accuracy improving by 37.6%, and the MAE decreasing from 0.2 to 0.113, an improvement of 43.5%. The LSTM neural network was slightly inferior to the AR-ANN, but it also showed an excellent correction effect.

For component v , it generally showed similar characteristics to the component u ; however, the fit of the original data was better, and the correlation coefficient with the observed data was already greater than 0.8. From the final results, the AR-ANN reduced the RMSE from 0.176 to 0.153, while LSTM had the best ability to reduce the MAE from 0.173 to 0.147. In Figure 9, there is a clear correction at the crest of the velocity curve, while at the trough, the revised results appear to deviate even more from the true value. This phenomenon was mostly expressed by the MLP and AR-ANN models, which illustrates the sensitivity of both algorithms to amplitude errors and the attendant disadvantages of instability.

Comparing the correction results of u and v , we found that the correction effect of deep learning on the meridional component was not very satisfactory. On the one hand, there was less room for the correction of deep learning methods in component v . On the other hand, any other factors, but the tide were ignored in the numerical simulations, while the wind may affect the ADCP results used for the comparison and feature extraction. These serendipity factors limit the enhancement effect of deep learning methods, which can be demonstrated in the final corrected results, where the R values still did not exceed 0.9 and the RMSE values were still not less than 0.15.

All the measured data were corrected and analyzed in the form of a Taylor function distribution. The figures show the correlation coefficient (R), root-mean-squared error (RMSE), and standard deviation (STD) of the model.

It can be seen from Figure 10 that the calibrated data from the three deep learning algorithms were very similar to the observed data in all metrics, and the AR-ANN model worked better in terms of the RMSE, which was similar to the LSTM and significantly better than the MLP. The R value between the original simulated data and the observed data was about 0.5; however, after correction, it was greater than 0.8, and the correlation of the AR-ANN model data was the highest, close to 0.9. The STD of the original simulated data did not exceed 0.2, which was much smaller than the observation, indicating that the

simulation underestimated in terms of tidal amplitude. The STDs of MLP and the AR-ANN were similar; both were closer to the observed data than the LSTM model, demonstrating the superiority of these two models in tidal velocity amplitude deviation correction again.

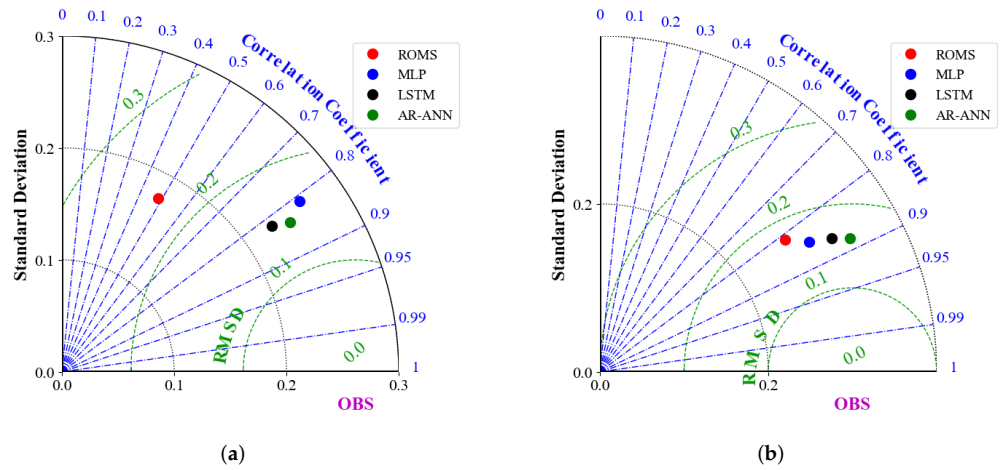


Figure 10. Taylor diagram for tidal current speed comparing estimation runs’ statistics for the R, RMSE, and STD of various models. (a) Taylor diagram of tidal current speed u; (b) Taylor diagram of tidal current speed v.

4. Tidal Current Energy Assessment

The proposed model was applied to the tidal energy assessment, and its effectiveness was verified. The power density is commonly used to measure the tidal energy, and its magnitude is mainly limited by the speed of the tidal current. The specific formula is as follows:

$$P = \frac{1}{2}\rho(\sqrt{u^2 + v^2})^3 \tag{21}$$

where P is the tidal power density and ρ is the density of seawater, and the value is taken as 1025 kg/m^3 .

Based on the three models proposed above, the tidal current energy density was calculated using the corrected data. The results of the correlational analysis are set out in Figure 11. The deep learning methods effectively improved the accuracy of tidal energy assessment. Furthermore, it can be found that the AR-ANN algorithm had the highest accuracy and best performance, with the correlation coefficient increased from around 0.3 to almost 0.8. It is worth noting that the STDs of the three modified assessments were also closer to the true values than the original data.

Detailed comparison results (RMSE, MAE, and R evaluation) of the tidal current energy assessment are illustrated in Table 3. In terms of the RMSE, the values of the three models were 50.096, 49.003, and 43.315, respectively. Compared to the original value of 74.68, the three methods reduced the error by 32.9%, 34.4%, and 42%, respectively. In the evaluation of the tidal energy, the deep learning methods had advantages in evaluating the tidal energy and showed superior results.

Table 3. Error metric for tidal current energy.

Metric	ROMS	MLP	LSTM	AR-ANN
RMSE	74.68	50.096	49.003	43.315
MAE	67.467	43.834	39.505	38.389
R	0.297	0.714	0.743	0.786

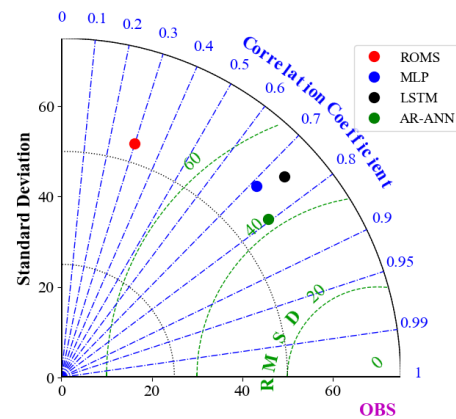


Figure 11. Taylor diagram for tidal current energy power density comparing estimation runs' statistics for the R, RMSE, and STD of various models.

5. Conclusions

In this paper, we proved the effectiveness of using deep learning methods for tidal current prediction. The three algorithms significantly reduced the amplitude and phase errors, both in the meridional and latitudinal components of velocity. In previous research, the use of numerical models for tidal currents' analysis has suffered from accuracy problems, while relying solely on deep learning methods would have faced shortcomings in long-time prediction. Ours is a model that combines the advantages of both, achieving the long-time prediction of tidal velocity and high accuracy assessment of tidal energy, which provides a new approach to the study of tidal current movement.

Comparative investigations were carried out to analyze the working mechanisms of different types of neural networks and find the most suitable one. Through the data analysis evaluations, it is clear that the AR-ANN model had the best performance, followed by LSTM, while MLP was the worst. However, LSTM requires a shorter training time and is more stable than the AR-ANN, which reveals where LSTM excels. In the treatment of different cases, AR-ANN is more sensitive to the amplitude error of the tidal velocity, while LSTM is effective in improving the phase error. This finding provides a reference for the subsequent selection of suitable deep learning networks according to the tidal velocity prediction characteristics. It also provides guidance for the following construction of more optimal neural networks for specific problems.

The proposed method contributes to high accuracy for tidal current energy resource assessment and high efficiency for tidal current energy extraction devices. It is also meaningful to determine the suitable location for energy generation and tidal turbine design. Equally important, it can also be used for the numerical simulation results of other ocean variables such as temperature, salinity, and sea surface height.

It is worth pointing out that the results likewise revealed the limitations of the proposed model. The effects of other forcings such as wind were not taken into account in the numerical simulation, and this inconsistency with the physical laws in the observation will constrain the power of deep learning methods. How to address the disruptions caused by these factors and explore the seasonal variability of tidal currents may be one of the issues to be solved in the future. Further research in this field would be of great help in combining the harmonic analysis with deep learning methods to develop more detailed and simpler tidal velocity simulation models and tidal energy assessment methods. Improving deep learning methods to build faster and more robust neural networks adapted to the characteristics of tidal current movements is also one of the priorities of future research.

Author Contributions: Conceptualization, H.W. (He Wu); Methodology, K.Z.; Software, X.Z. and L.Z.; Validation, Y.F. and X.W.; Data collection, L.Z.; Data analysis, Y.F.; Writing-original draft preparation, K.Z.; Writing-review and editing, H.W. (He Wu), X.Z. and H.W. (Haifeng Wang); Supervision, X.W. and X.Z.; Funding acquisition, H.W. (Haifeng Wang). All authors have read and agreed to the published version of the manuscript.

Funding: This research was funded by National Natural Science Foundation of China (Grant No. 42276228) and the National Key Research and Development Program of China “Cooperative study on comprehensive evaluation methods of wave and tidal currents energy technology” (2019YFE0102500).

Institutional Review Board Statement: Not applicable.

Informed Consent Statement: Not applicable.

Data Availability Statement: Not applicable.

Conflicts of Interest: The authors declare no conflict of interest.

Abbreviations

The following abbreviations are used in this manuscript:

OBS	Observation
MLP	Multilayer perceptron
LSTM	Long-short term memory
AR-ANN	Attention-ResNet neural network
ROMS	Regional Ocean Modeling System
ADCP	Acoustic Doppler current profiler

References

- Li, B.; Chen, W.; Li, J.; Liu, J.; Shi, P. Integrated monitoring and assessments of marine energy for a small uninhabited island. *Energy Rep.* **2022**, *8*, 63–72. [[CrossRef](#)]
- Liu, X.; Chen, Z.; Si, Y.; Qian, P.; Wu, H.; Cui, L.; Zhang, D. A review of tidal current energy resource assessment in China. *Renew. Sustain. Energy Rev.* **2021**, *145*, 111012. [[CrossRef](#)]
- Burić, M.; Grgurić, S.; Mikulčić, H.; Wang, X. A numerical investigation of tidal current energy resource potential in a sea strait. *Energy* **2021**, *234*, 121241. [[CrossRef](#)]
- Uihlein, A.; Magagna, D. Wave and tidal current energy—A review of the current state of research beyond technology. *Renew. Sustain. Energy Rev.* **2016**, *58*, 1070–1081. [[CrossRef](#)]
- Bryden, I.G.; Couch, S.J. How much energy can be extracted from moving water with a free surface: A question of importance in the field of tidal current energy? *Renew. Energy* **2007**, *32*, 1961–1966. [[CrossRef](#)]
- Zhang, J.; Moreau, L.; Machmoum, M.; Guillermin, P.-E. State of the art in tidal current energy extracting technologies. In Proceedings of the 2014 First International Conference on Green Energy ICGE 2014, Sfax, Tunisia, 25–27 March 2014; pp. 1–7. [[CrossRef](#)]
- Marsh, P.; Penesis, I.; Nader, J.R.; Cossu, R.; Auguste, C.; Osman, P.; Couzi, C. Tidal current resource assessment and study of turbine extraction effects in Banks Strait, Australia. *Renew. Energy* **2021**, *180*, 1451–1464. [[CrossRef](#)]
- Pawlowicz, R.; Beardsley, B.; Lentz, S. Classical tidal harmonic analysis including error estimates in MATLAB using T_TIDE. *Comput. Geosci.* **2002**, *28*, 929–937. [[CrossRef](#)]
- Nachtane, M.; Tarfaoui, M.; Goda, I.; Rouway, M. A review on the technologies, design considerations and numerical models of tidal current turbines. *Renew. Energy* **2020**, *157*, 1274–1288. [[CrossRef](#)]
- Garrett, C.; Cummins, P. Limits to tidal current power. *Renew. Energy* **2008**, *33*, 2485–2490. [[CrossRef](#)]
- Darwin, G.H. Ellipsoidal Harmonic Analysis. *Philos. Trans. R. Soc. Lond. Ser. A* **1901**, *197*, 461–557.
- Sarkar, D.; Osborne, M.; Adcock, T. A Machine Learning Approach to the Prediction of Tidal Currents. In Proceedings of the 26th International Ocean and Polar Engineering Conference, Rhodes, Greece, 26 June–2 July 2016.
- Foreman, M.G.G.; Cherniawsky, J.Y.; Ballantyne, V.A. Versatile Harmonic Tidal Analysis: Improvements and Applications. *J. Atmos. Ocean. Technol.* **2009**, *26*, 806–817. [[CrossRef](#)]
- Niwa, Y.; Hibiya, T. Generation of baroclinic tide energy in a global three-dimensional numerical model with different spatial grid resolutions. *Ocean Model.* **2014**, *80*, 59–73. [[CrossRef](#)]
- Freitas, C. The issue of numerical uncertainty. *Appl. Math. Model.* **2002**, *26*, 237–248. [[CrossRef](#)]
- Yao, J.; Wu, W.; Zhao, Z. Motion and Load Prediction of Floating Platform in South China Sea Using Deep Learning and Prototype Monitoring Information. In Proceedings of the ASME 2019 38th International Conference on Ocean, Offshore and Arctic Engineering, Volume 3: Structures, Safety, and Reliability, Glasgow, UK, 9–14 June 2019; p. V003T02A014. [[CrossRef](#)]

17. Najafzadeh, M.; Oliveto, G. Scour Propagation Rates around Offshore Pipelines Exposed to Currents by Applying Data-Driven Models. *Water* **2022**, *14*, 493. [[CrossRef](#)]
18. Najafzadeh, M.; Oliveto, G.; Saberi-Movahed, F. Estimation of Scour Propagation Rates around Pipelines While Considering Simultaneous Effects of Waves and Currents Conditions. *Water* **2022**, *14*, 1589. [[CrossRef](#)]
19. Chen, X.; Yu, R.; Ullah, S.; Wu, D.; Li, Z.; Li, Q.; Qi, H.; Liu, J.; Liu, M.; Zhang, Y. A novel loss function of deep learning in wind speed forecasting. *Energy* **2022**, *238*, 121808. [[CrossRef](#)]
20. Dimililer, K.; Dindar, H.; Al-Turjman, F. Deep learning, machine learning and internet of things in geophysical engineering applications: An overview. *Microprocess. Microsyst.* **2021**, *80*, 103613. [[CrossRef](#)]
21. Sarkar, D.; Osborne, M.A.; Adcock, T.A.A. Prediction of tidal currents using Bayesian machine learning. *Ocean Eng.* **2018**, *158*, 221–231. [[CrossRef](#)]
22. Kavousi-Fard, A.; Su, W. A Combined Prognostic Model Based on Machine Learning for Tidal Current Prediction. *IEEE Trans. Geosci. Remote Sens.* **2017**, *55*, 3108–3114. [[CrossRef](#)]
23. Zhang, A.; Lin, Y.; Sun, Y.; Yuan, H.; Wang, M.; Liu, G.; Hu, Y. Tidal current prediction based on fractal theory and improved least squares support vector machine. *IET Renew. Power Gener.* **2022**, *16*, 389–401. [[CrossRef](#)]
24. Riazi, A. Accurate tide level estimation: A deep learning approach. *Ocean Eng.* **2020**, *198*, 107013. [[CrossRef](#)]
25. Yang, C.-H.; Wu, C.-H.; Hsieh, C.-M. Long Short-Term Memory Recurrent Neural Network for Tidal Level Forecasting. *IEEE Access* **2020**, *8*, 159389–159401. [[CrossRef](#)]
26. Bayindir, C. Predicting the Ocean Currents using Deep Learning. *arXiv* **2019** arXiv:1906.08066.
27. Sarkar, D.; Osborne, M.A.; Adcock, T.A.A. Spatiotemporal prediction of tidal currents using Gaussian processes. *J. Geophys. Res. Ocean.* **2019**, *124*, 2697–2715. [[CrossRef](#)]
28. Feng, B.; Qian, P.; Si, Y.; Liu, X.; Yang, H.; Wen, H.; Zhang, D. Comparative Investigations of Tidal Current Velocity Prediction Considering Effect of Multi-Layer Current Velocity. *Energies* **2020**, *13*, 6417. [[CrossRef](#)]
29. Aly, H.H.H. Intelligent optimized deep learning hybrid models of neuro wavelet, Fourier Series and Recurrent Kalman Filter for tidal currents constitutions forecasting. *Ocean Eng.* **2020**, *218*, 108254. [[CrossRef](#)]
30. Shchepetkin, A.F.; McWilliams, J.C. The regional oceanic modeling system (ROMS): A split-explicit, free-surface, topography-following-coordinate oceanic model. *Ocean Model.* **2005**, *9*, 347–404. [[CrossRef](#)]
31. Moore, A.M.; Arango, H.G.; Broquet, G.; Powell, B.S.; Weaver, A.T.; Zavala-Garay, J. The Regional Ocean Modeling System (ROMS) 4-dimensional variational data assimilation systems: Part I—System overview and formulation. *Prog. Oceanogr.* **2011**, *91*, 34–49. [[CrossRef](#)]
32. Jung, K.; Cho, Y.K.; Tak, Y.J. Containers and orchestration of numerical ocean model for computational reproducibility and portability in public and private clouds: Application of ROMS 3.6. *Simul. Model. Pract. Theory* **2021**, *109*, 102305. [[CrossRef](#)]
33. Bradbury, M.C.; Conley, D.C. Using Artificial Neural Networks for the Estimation of Subsurface Tidal Currents from High-Frequency Radar Surface Current Measurements. *Remote Sens.* **2021**, *13*, 3896. [[CrossRef](#)]
34. Guo, H.; Guo, C.; Xu, B.; Xia, Y.; Sun, F. MLP neural network-based regional logistics demand prediction. *Neural Comput. Appl.* **2021**, *33*, 3939–3952. [[CrossRef](#)]
35. Zhou, K.; Yu, H.; Zhao, W.X.; Wen, J.-R. Filter-enhanced MLP is All You Need for Sequential Recommendation. In Proceedings of the ACM Web Conference 2022, Lyon, France, 25–29 April 2022; pp. 2388–2399. [[CrossRef](#)]
36. Bai, L.-H.; Xu, H. Accurate estimation of tidal level using bidirectional long short-term memory recurrent neural network. *Ocean Eng.* **2021**, *235*, 108765. [[CrossRef](#)]
37. Zhang, Z.; Hou, M.; Zhang, F.; Edwards, C.R. An LSTM based Kalman Filter for Spatio-temporal Ocean Currents Assimilation. In Proceedings of the International Conference on Underwater Networks & Systems, Atlanta, GA, USA, 23–25 October 2019; pp. 1–7. [[CrossRef](#)]
38. Vaswani, A.; Shazeer, N.; Parmar, N.; Uszkoreit, J.; Jones, L.; Gomez, A.N.; Kaiser, L.; Polosukhin, I. Attention is all you need. In Proceedings of the Advances in Neural Information Processing Systems, Long Beach, CA, USA, 4–9 December 2017; Volume 30.
39. Xu, Q.S.; Yang, X.H.; Huang, X. Ensemble Residual Networks for Short Term Load Forecasting. *IEEE Access* **2020**, *8*, 64750–64759. [[CrossRef](#)]

Disclaimer/Publisher’s Note: The statements, opinions and data contained in all publications are solely those of the individual author(s) and contributor(s) and not of MDPI and/or the editor(s). MDPI and/or the editor(s) disclaim responsibility for any injury to people or property resulting from any ideas, methods, instructions or products referred to in the content.